

Supporting Information

A new strategy for integrating semiconducting SWCNTs into pseudo-cubic In₂O₃ heterostructures for solid-state symmetric supercapacitors with a superior stability and specific-capacitance

Rajneesh Kumar Mishra^a, Jae Hyeon Ryu^a, Hyuck-In Kwon^{b*}, and Sung Hun Jin^{a*}

^aDepartment of Electronic Engineering, Incheon National University, Incheon 406-772, Republic of Korea.

^bSchool of Electrical and Electronics Engineering, Chung-Ang University, Seoul 156-756, Republic of Korea.

*Professor Sung Hun Jin, E-mail: shjin@inu.ac.kr, Fax: +82-32-835-0774, Tel: +82-32-835-8865; Professor Hyuck-In Kwon, E-mail: hyuckin@cau.ac.kr.

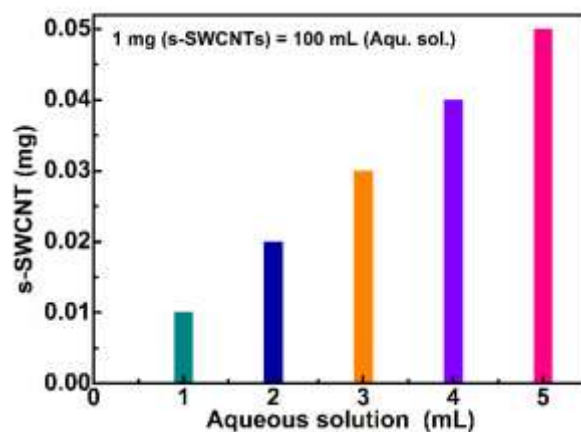


Fig. S1: Analytically estimated mass of s-SWCNTs vs split aqueous volume. The aqueous solution volume (mL) was used as it is received from Nanointegris Technologies, Inc. during hydrothermal synthesis of heterostructures of $\text{In}_2\text{O}_3/\text{s-SWCNTs}$.

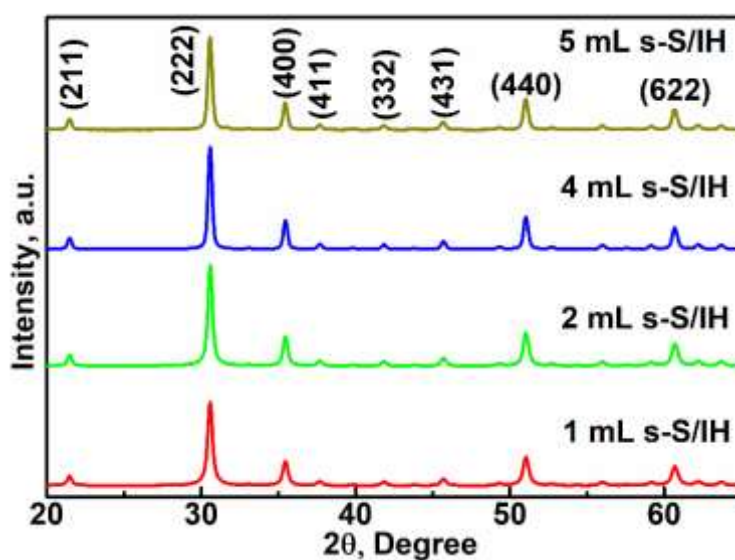


Fig. S2. Typical XRD patterns of s-S/IH.

Table S1: Structural parameters of s-S/IH.

Samples	2 θ (Degree)	“d” spacing	Planes	Lattice parameters
In ₂ O ₃ nanocube	21.4623	0.4136	(211)	a (b = c) = 10.1238 Å
	30.5244	0.2926	(222)	
	35.4388	0.2530	(400)	
	51.0111	0.1788	(440)	
	60.6562	0.1525	(622)	
1 mL s-S/IH				
1 mL s-S/IH	21.4720	0.4134	(211)	a (b = c) = 10.1198 Å
	30.5721	0.2922	(222)	
	35.4519	0.2529	(400)	
	51.0333	0.1788	(440)	
	60.6730	0.1525	(622)	
2 mL s-S/IH				
2 mL s-S/IH	21.4727	0.4134	(211)	a (b = c) = 10.1175 Å
	30.5796	0.2921	(222)	
	35.4600	0.2529	(400)	
	51.0355	0.1788	(440)	
	60.6952	0.1525	(622)	
3 mL s-S/IH				
3 mL s-S/IH	21.4711	0.4135	(211)	a (b = c) = 10.1165 Å
	30.5721	0.2921	(222)	
	35.4639	0.2529	(400)	
	51.0370	0.1788	(440)	
	60.6758	0.1525	(622)	
4 mL s-S/IH				
4 mL s-S/IH	21.4678	0.4135	(211)	a (b = c) = 10.1195 Å
	30.5646	0.2922	(222)	
	35.4530	0.2529	(400)	
	51.0272	0.1788	(440)	
	60.6687	0.1525	(622)	
5 mL s-S/IH				
5 mL s-S/IH	21.4724	0.4134	(211)	a (b = c) = 10.1218 Å
	30.5691	0.2922	(222)	
	35.4446	0.2530	(400)	
	51.0153	0.1789	(440)	
	60.6572	0.1525	(622)	

The lattice spacing (d) has been calculated by the Bragg's diffraction formula:

$$2d \sin \theta = n\lambda$$

where θ is the Bragg's diffraction angle and λ is the wavelength of x-ray.

The lattice parameters ($a = b = c$) have been estimated by following equation:

$$d = \frac{a}{\sqrt{(h^2)+(k^2)+(l^2)}}$$

where (hkl) is the crystal planes of the In_2O_3 nanostructure.

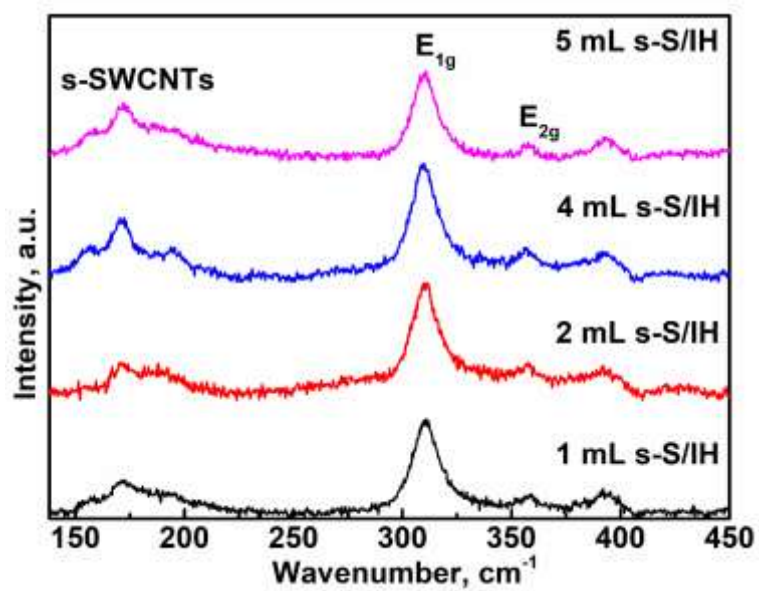


Fig. S3: Raman spectra of s-S/IH.

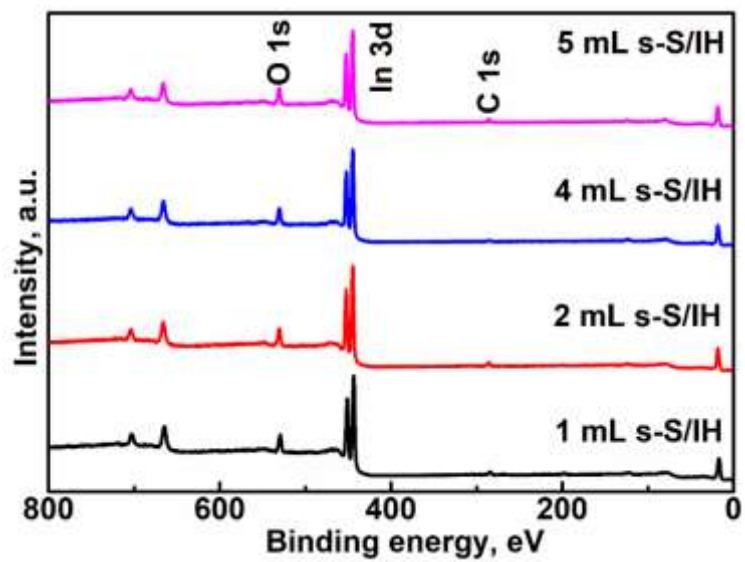


Fig. S4: Typical XPS spectra of s-S/IH.

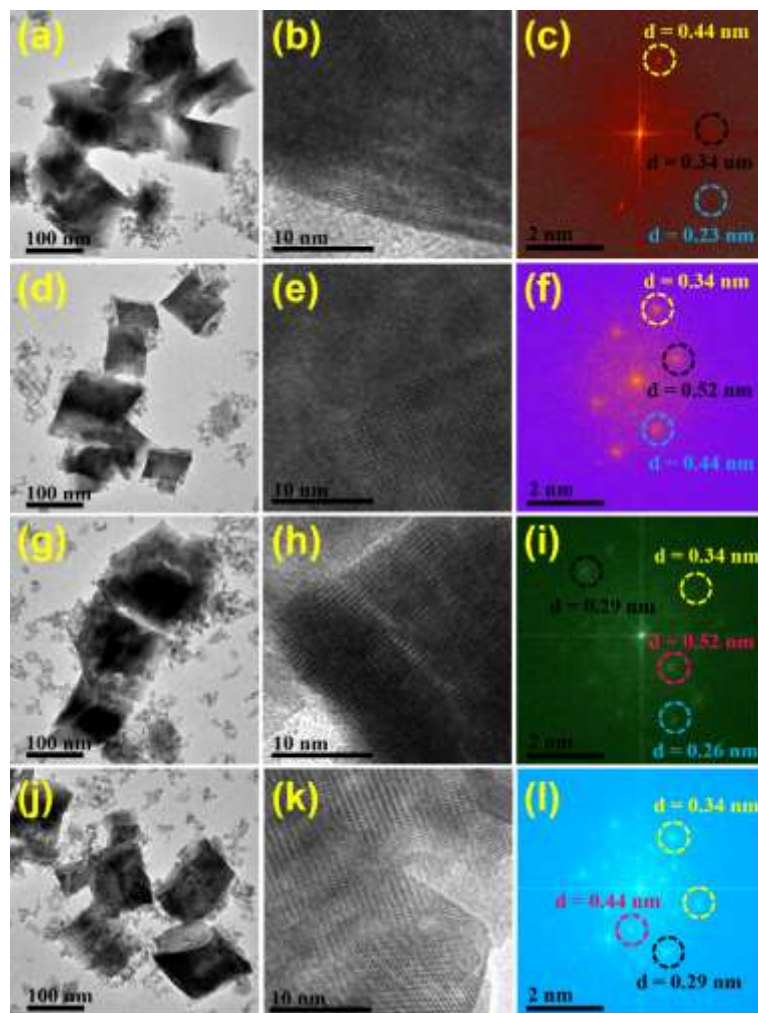


Fig. S5: TEM, HRTEM images and corresponding FFT of 1 mL (a-c), 2 mL (d-f), 4 mL (g-i) and 5 mL (j-l) s-S/IH.

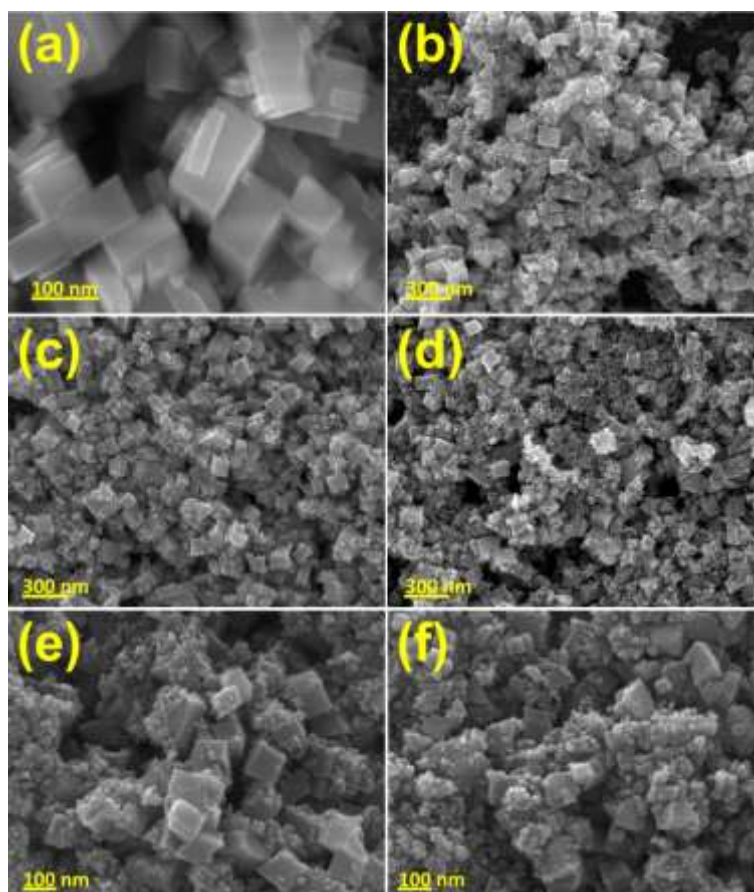


Fig. S6: FESEM images of (a) In₂O₃ nanocube, (b) 1 mL, (c) 2 mL, (d) 3 mL, (e) 4 mL and (f) 5 mL s-S/IH.

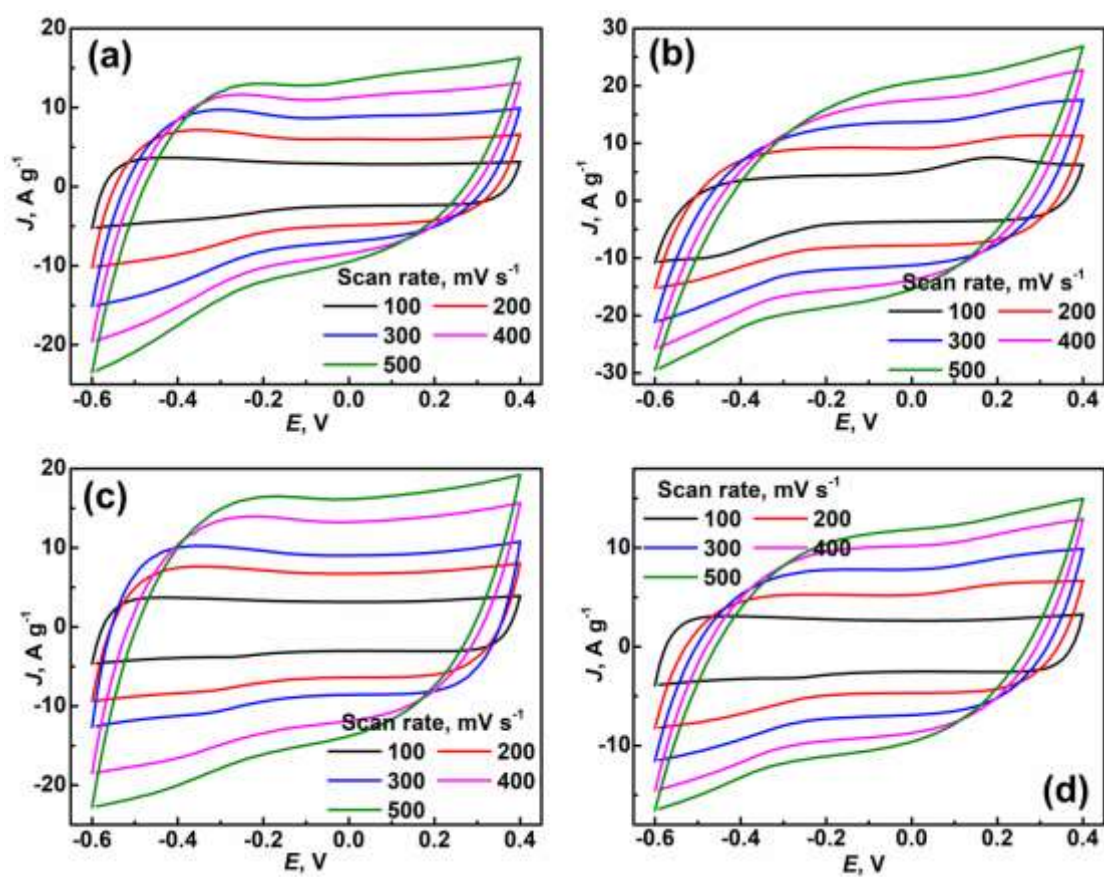


Fig. S7: CV plots of (a) 1 mL, (b) 2 mL, (c) 4 mL and (d) 5 mL s-S/IH based supercapacitor electrodes at different scan rates.

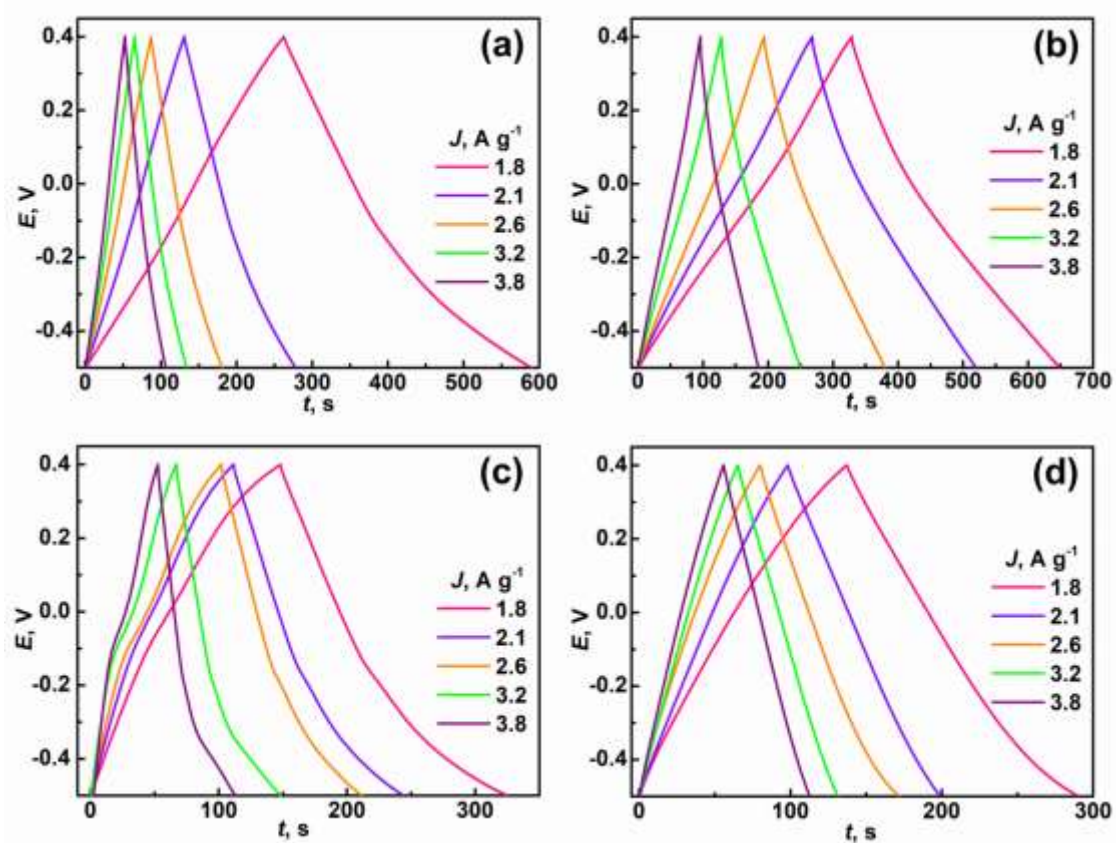


Fig. S8: GCD profiles of (a) 1 mL, (b) 2 mL, (c) 4 mL and (d) 5 mL s-S/IH based supercapacitor electrodes at various current densities.

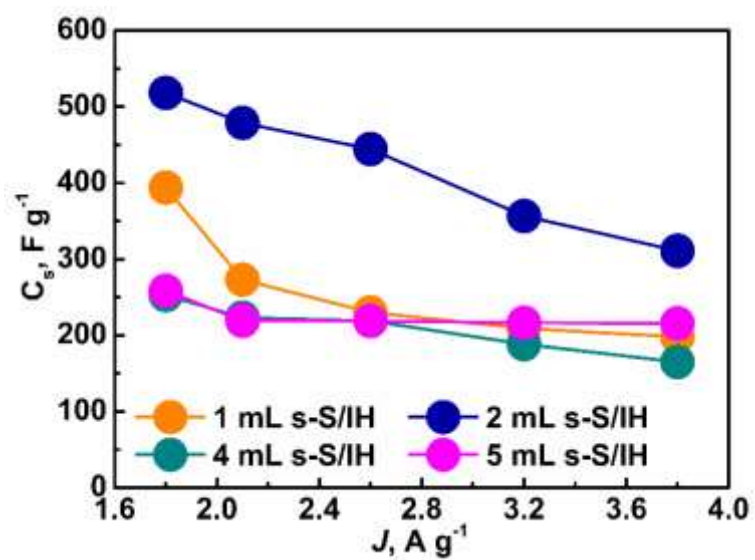


Fig. S9: Specific capacitance at various current densities of s-S/IH based supercapacitor electrodes.

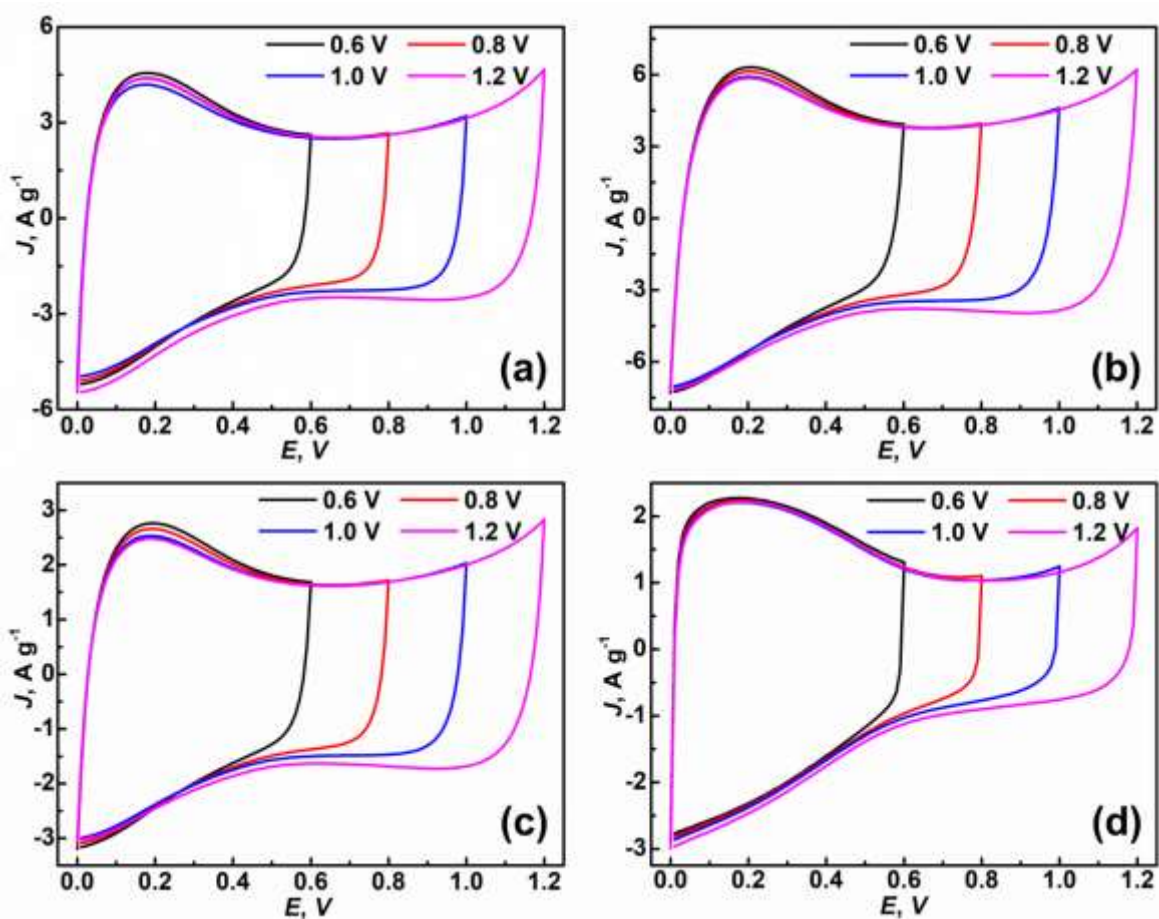


Fig. S10: CV curves (scan rate 50 mV s^{-1}) of the (a) 1 mL, (b) 2 mL, (c) 4 mL, and (d) 5 mL s-S/IH based SSCs measured at different scan voltage window.

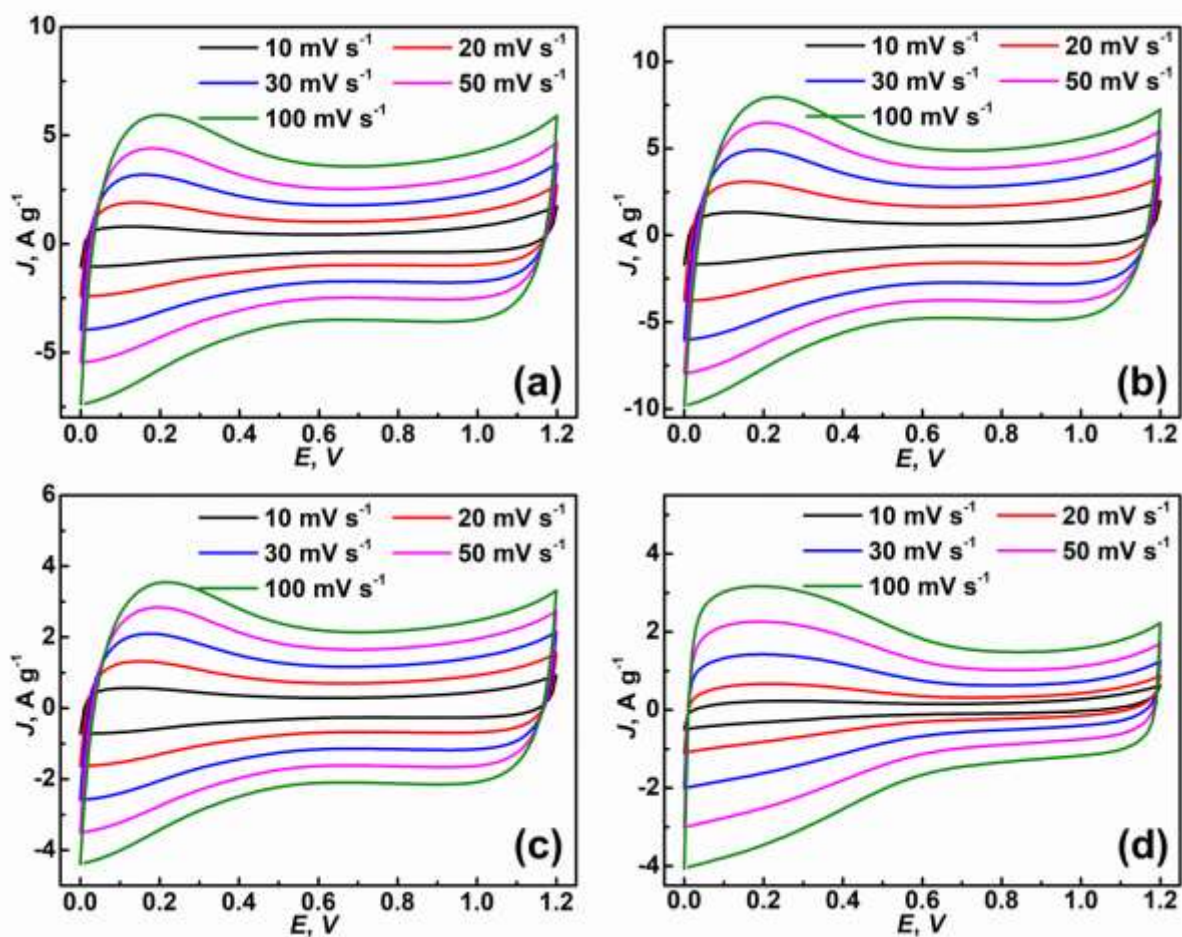


Fig. S11: CV curves of the (a) 1 mL, (b) 2 mL, (c) 4 mL, and (d) 5 mL s-S/IH based SSCs observed at different scan rates.

Interestingly, we studied the energy efficiency, which was evaluated by area under the GCD plots [Fig. 8(e and f)] to investigate, whether possible reaction on electrodes are reversible in nature or not.

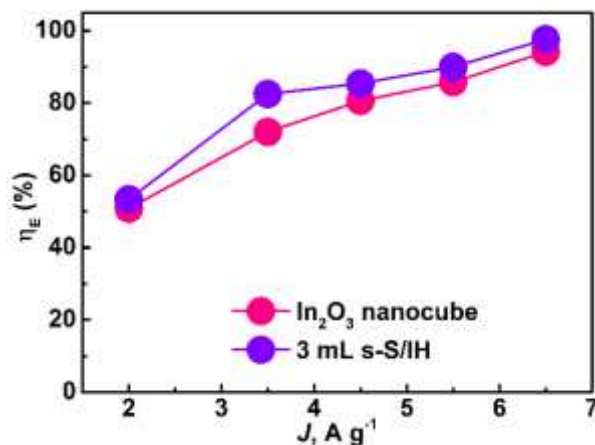


Fig. S12: Energy efficiency vs different current density plot of bare In₂O₃ nanocube and 3 mL s-S/IH based SSC devices.

We evaluated the energy efficiency at different current densities of GCD plots (SSC device) from Fig. 8 (e and f) and results are illustrated in Fig. S12. For, non-ideal GCD plots, the energy efficiency (η_E) can be evaluated by the following Eq. S2 [3, 4]:

$$\eta_E = E_{int/D} / E_{int/C} \quad \dots\dots\dots S2$$

where $E_{int/D} = I \int_{t(U_{max})}^{t(U_{min})} U(t) dt$ and $E_{int/C}$ are the discharge and charge energies respectively.

From Fig. S12, the calculated energy efficiency is estimated to be 50.8 %, 71.9 %, 80.6 %, 85.7 % and 94.1 % for bare In₂O₃ based SSC device, whereas for 3 mL s-S/IH based SSC device, were extracted as 53.3, 82.5, 85.4, 89.9 and 97.6 % at current densities of 2 A g⁻¹, 3.5 A g⁻¹, 4.5 A g⁻¹, 5.5 A g⁻¹ and 6.5 A g⁻¹, respectively. Hence, in the typical electrical double-layer capacitors (EDLC), one of reasons why energy efficiency loss was observed, could be ascribed to the heat dissipation [4]. Thus, at low current density (2 A g⁻¹), the SSC devices show

both electric double layer and pseudo capacitive behavior, denoting that the system is irreversible, whereas at high current densities, the system is reversible supported by the evidence of a triangular shape of GCD plots. This irreversible process may be due to s-SWCNT/In₂O₃ heterostructures. Additionally, in the case of involving faradaic charge storage, when the low energy efficiency is less than 50%, the system is evidently regarded as being involved in the irreversible faradaic processes. Also, decomposition products, which are constituted in the supercapacitor electrodes, partially block the porosity and dominating to alter the EDLC characteristics [4].

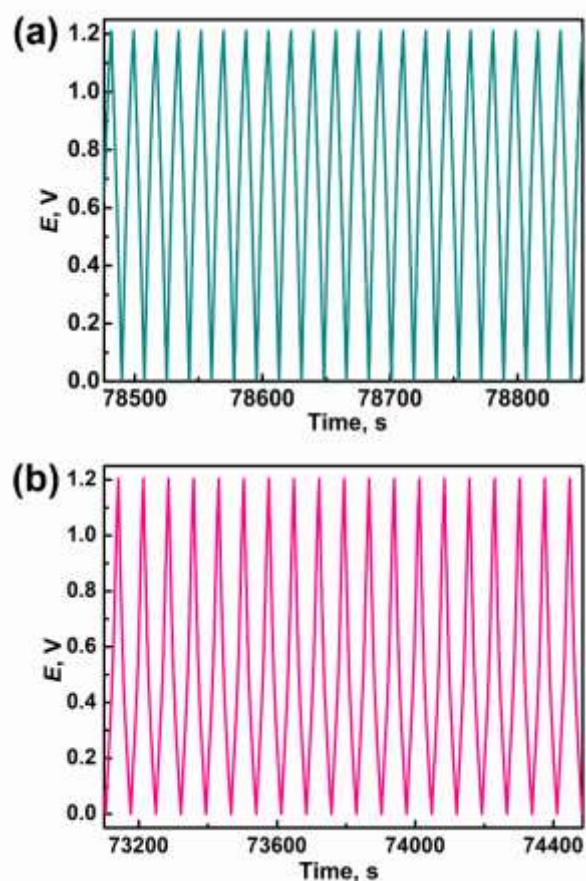


Fig. S13: In between GCD cycles during stability test of the (a) bare In₂O₃ nanocube and (b) 3 mL s-S/IH based SSCs (Current density 4.5 A g⁻¹).

For the better understanding of reproducible nature of our assembled 3 mL SSC device, we have tested long-term cycling stability of two similar devices. It is observed that our assembled 3 mL SSC device shows excellent reproducibility over 5000 cycles for two SSC devices and the results are depicted in Fig. 9(c), Fig. S13(b) and Fig. S14. Fig. 14(a-c) represents the 1st, 1000th and 5000th cycles of two devices whereas Fig. 14(d) elucidate the statistical analyses with error bar. All the estimated results are well matched and consistent and acceptable data accuracy with 3.91% standard deviation in consideration of sample variation and measurement system resolution. The standard deviation (SD) was evaluated by using the statistical relation and discussed in literature [5].

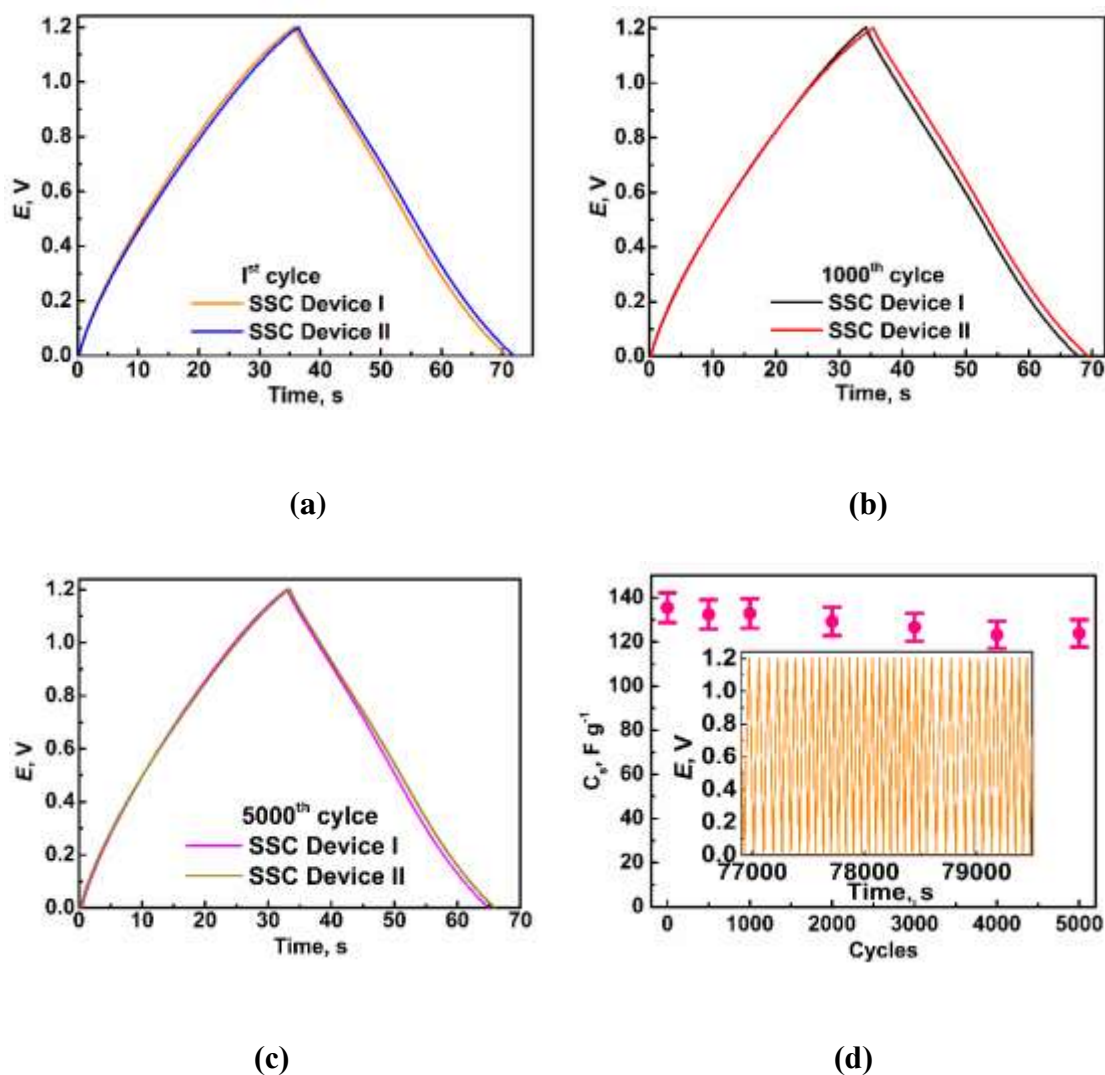


Fig. S14: Reproducibility analyses for two ensembles of 3 mL s-S/IH based SSC; (a) 1st cycles, (b) 1000th cycles, (c) 5000th cycles, and (d) long-term stability with statistical error bar (inset show in between GCD cycles during stability test) of 3 mL s-S/IH based SSCs during long-term stability (Current density 4.5 A g⁻¹).

Furthermore, we studied the self-discharge measurements and accelerate ageing tests (cycling + floating + self-discharge) in the potentiostatic mode for 3 mL s-S/IH based SSC devices at three specific voltages such as 0.8 V, 1.0 V and 1.2 V respectively, as shown in Fig. S15. The cycling (4 cycles) at constant current density of 4.5 A g⁻¹, floating (3 h) also called accelerated

ageing and self-discharge 2 h of potentiostatic mode were examined for 60 h for the better understanding of long-term durability and to validate the cycling (GCD) stability results as shown in Fig. 9(c) of the assembled s-S/IH based SSC devices.

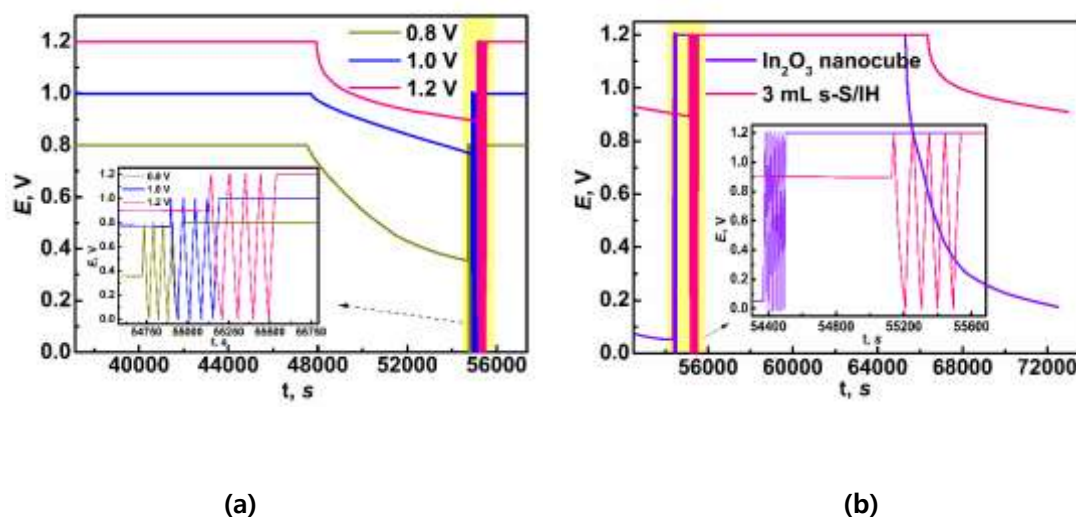


Fig. S15: Accelerate aging (floating) for 3 h, self-discharge behavior for 2 h and charge/discharge cycling (4 cycles) of 3 mL s-S/IH based SSC device (a) and a comparative analysis for both the bare In_2O_3 nanocube and 3 mL s-S/IH based SSC devices at a constant voltage (1.2 V) (b), during long-term durability test.

Additionally, we performed a new method for the stability of SSC device that combines the common cycling method, comprising of galvanostatic charge/discharge measurements, with a floating and self-discharge test which is carried out at three constant voltages such as 0.8 V, 1.0 V and 1.2 V during predefined time as shown in Fig. S15. The accelerated ageing behavior of SSC devices based on cycling, floating and self-discharge method, showed excellent stability for 60 h at three different voltage such as 0.8 V, 1.0 V and 1.2 V, respectively.

In addition, the self-discharge demonstration is a vital feature for a better understanding of the assembled SSC devices. Fig. S15 (a) shows self-discharge curves (2 h) after cycling (4

cycles) and floating (3 h) at three constant voltages (0.8, 1.0 and 1.2 V) as function of time. Thus, 3 mL s-S/IH based SSC device depicts the reduced self-discharge rate with a small voltage decrease over time, illustrates outstanding results without forgetting the high specific capacitance and excellent stability. Furthermore, Fig. S15(b) shows the compared results of bare In_2O_3 nanocube and 3 mL s-S/IH based SSC devices at constant voltage of 1.2 V. It is observed that 3 mL s-S/IH based SSC devices is more durable than the bare In_2O_3 nanocube based SSC devices. In addition, the reduced self-discharge characteristics observed may due to different contributions like as parasitic faradaic reactions, charge re-distribution, corrosion process, ion transport limitations and ohmic leakages or even several of these contributions combined [6-9]. Therefore, it validates the long-term stability studied by GCD cycling as shown in Fig. 9 (c) for bare In_2O_3 nanocube and 3 mL s-S/IH based assembled SSC devices. This is another confirmation of the very stable performance of the 3 mL s-S/IH based assembled SSC device developed in this study, despite GCD cycling stability.

Interestingly, the leakage current of 3 mL s-S/IH based SSC device was also recorded during each 3 h floating period, the leakage current profile during one potentiostatic sequence at three constant voltages 0.8, 1.0 and 1.2 V respectively, is shown in Fig. S16. Once the 3 mL s-S/IH based SSC is fully charged, the leakage current quickly decreases within few minutes, followed by reaching at a thermal equilibrium as it goes forward a longer time as depicted in Fig. S16. It is observed that a leakage current was reduced with a reduced constant voltage, which can be explained by double layer structure with a diffusion layer, where ions have weak interactions with the symmetric SSC device electrodes, and a compact layer with ions stalwartly interacting with the electrode. Initially, the ions in the bulk, flowing toward the diffusion layer, consequences in a drastic decay of current. After that, the ions in the diffusion layer are pushed to be a compact layer, until the structure of the electrical double layer is

ordered, leading to an equilibrium state [7].

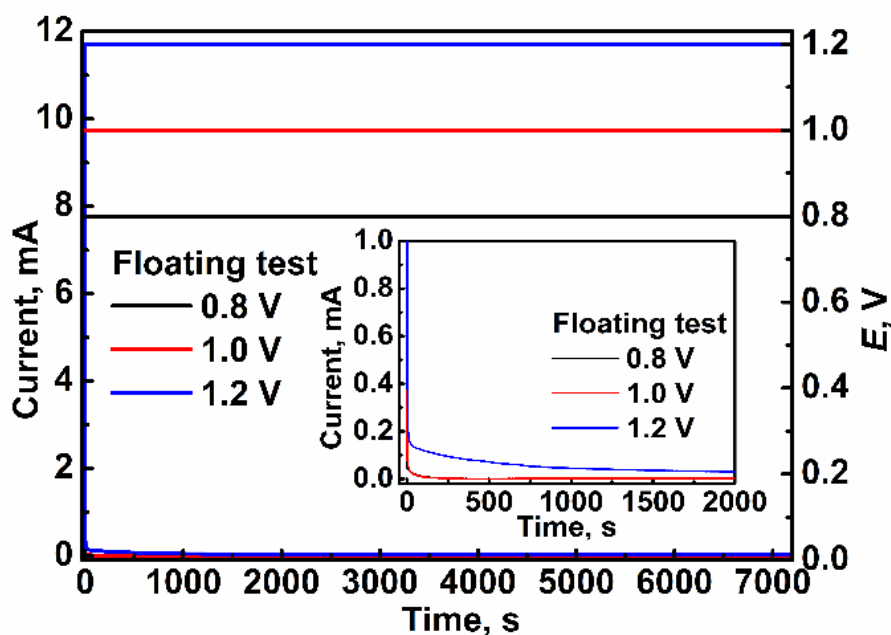


Fig. S16: Leakage current profile of 3 mL s-S/IH based SSC device at three voltages (0.8, 1.0, 1.2 V) during accelerate ageing (floating) for 3 h during long-term durability test.

Further, we tested EIS of 3 mL s-S/IH in the frequency range from 0.01 Hz to 10^5 Hz as shown in Fig. S17. The values of internal resistance (R_s) and charge transfer resistance (R_{ct}) are 3.5 Ω and 1.4 Ω (before 5000 GCD cycles) and 3.8 Ω and 1.5 Ω (after 5000 GCD cycles), respectively. These results show the increased internal and ionic resistances, compared with the data in the previous study before and after 5000 cycles under frequency range 1 Hz to 10^5 Hz as shown in Fig. 9(d).

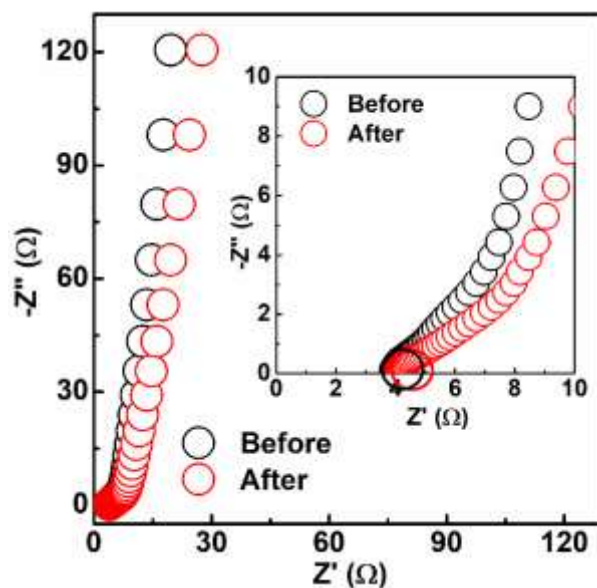


Fig. S17: Electrochemical impedance spectra of 3 mL s-S/IH based SSC devices (before and after 5000 cycles).

In this study, we used semiconducting single-walled carbon nanotubes (s-SWCNTs) for the synthesis of s-SWCNT/ In_2O_3 heterostructures (s-S/IH), which were directly purchased from “Nanointegris Inc.”. The s-SWCNTs, used in this work, have semiconducting properties with a purity (>99%) as commercially available. Based on the data sheet [10] which is available from the webpage, Nanointegris. Inc, a diameter distribution for s-SWCNTs ranges from 1.2 nm to 1.7 nm which contribute to the transitions in the range of ~ 0.7 -1.4 eV as shown in Fig. S18. Therefore, the transitions in the energy range 0.7-1.4 eV indicates that s-SWCNTs, in this study, correspond to the first, second and the third semiconducting transitions (closed symbols, E_{11}^S , E_{22}^S , E_{33}^S). Cheng et al. discussed the similar behavior in case of semiconducting SWNTs [11]. Therefore, it is rationally confident that all the carbon nanotubes in this study are expected to have semiconducting properties (> 99%) which are matched with the data sheet [10].

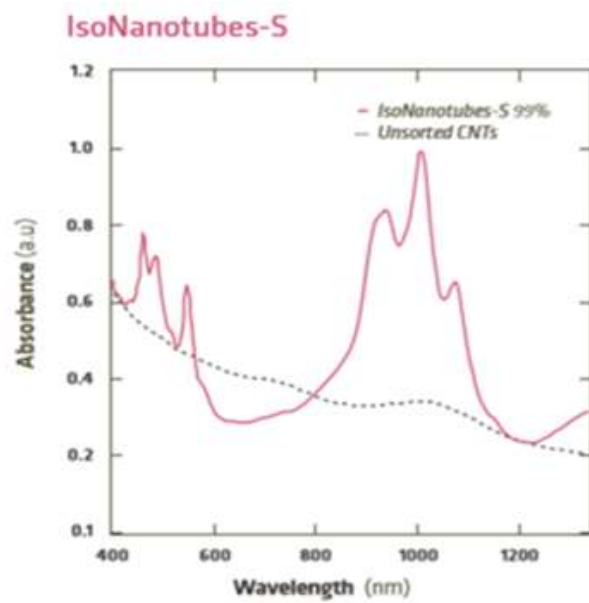


Fig. S18: Optical absorbance plots for IsoNanotubes-S (99%) [Ref. 10].

References

- [1] N. G. Pramod, S. N. Pandey, P. P. Sahay, Structural, optical and methanol sensing properties of sprayed In₂O₃ nanoparticle thin films, *Ceramics Int.*, 2012, **38**, 4151-4158.
- [2] R. K. Mishra, G. W. Baek, K. Kim, H.-In Kwon, S. H. Jin, One-step solvothermal synthesis of carnation flower-like SnS₂ as superior electrodes for supercapacitor applications, *App. Surf. Sci.*, 2017, 425, 923-931.
- [3] T. Brousse, D. Bélanger, Jeffrey W. Long, To be or not to be pseudocapacitive? *J. Electrochem. Soc.*, 2015, **162**, A5185-A5189.
- [4] A. Laheäär, P. Przygocki, Q. Abbas, F. Béguin, Appropriate methods for evaluating the efficiency and capacitive behavior of different types of supercapacitors, *Electrochem. Commun.*, 2015, **60**, 21-25.
- [5] R. K. Mishra, Ajay Kushwaha, P. P. Sahay, Influence of Cu doping on the structural, photoluminescence and formaldehyde sensing properties of SnO₂ nanoparticles, *RSC Adv.*, 2014, **4**, 3904-3912.
- [6] E. Frackowiak, P. Ratajczak and F. Béguin, Electrochemical Capacitors Based on Carbon Electrodes in Aqueous Electrolytes, *Adv. Electrochem. Sci. Engg., Book Ch. 8*, 2016, 285-312.
- [7] P. Ratajczak, K. Jurewicz, F. Béguin, Factors contributing to ageing of high voltage carbon/carbon supercapacitors in salt aqueous electrolyte, *J. Appl. Electrochem.*, 2014, **44**, 475-480.
- [8] A. J. Paleo, P. Staiti, A. Brigandi, F. N. Ferreira, A. M. Rocha, F. Lufrano, Supercapacitors based on AC/MnO₂ deposited onto dip-coated carbon nanofiber cotton fabric electrodes, *Energy Storage Mater.*, 2018, **12**, 204-215.
- [9] F. Béguin, E. Frackowiak, Supercapacitors: Materials, systems, and applications Wiley-

VCH cop., 2013.

[10] <http://nanointegris.com/wp-content/uploads/2017/10/Carbon-Nanotubes-Technical-Data-Sheet-1.pdf>.

[11] Q. Cheng, S. Debnath, E. Gregan, H. J. Byrne, Vibrational mode assignments for bundled single-wall carbon nanotubes using Raman spectroscopy at different excitation energies, 2011, **102**, 309-317.